ETH zürich

ETH Library

Exploitation of Cationic Silica Nanoparticles for Bioprinting of Large-Scale Constructs with High Printing Fidelity

Journal Article

Author(s):
Lee, Mihyun; Bae, Kraun; Guillon, Pierre; Chang, Jin; Arlov, Øystein; Zenobi-Wong, Marcy

Publication date:
2018-11

Permanent link:
https://doi.org/10.3929/ethz-b-000304153

Rights / license:
In Copyright - Non-Commercial Use Permitted

Originally published in:
ACS Applied Materials & Interfaces 10(44), https://doi.org/10.1021/acsami.8b13166

Funding acknowledgement:
173868 - Sinergia Project: A Tissue, Cell and Molecular Approach to Understanding and Treating Microtia (SNF)

This page was generated automatically upon download from the ETH Zurich Research Collection.
For more information, please consult the Terms of use.

Exploitation of Cationic Silica Nanoparticles for Bioprinting of Large-Scale Constructs with High Printing Fidelity

*Mihyun Lee[1], Kraun Bae[1], Pierre Guillon[1], Jin Chang[1], Øystein Arlov[2], Marcy Zenobi-Wong[1,]**

AUTHOR ADDRESS

[1]Tissue Engineering+Biofabrication Laboratory, Institute for Biomechanics, ETH Zürich, Otto-Stern-Weg 7, 8093 Zürich, Switzerland

[2]Department of Biotechnology and Nanomedicine, SINTEF Industry, Richard Birkelands vei 3B, 7034 Trondheim, Norway

*E-mail: marcy.zenobi@hest.ethz.ch

KEYWORDS Bioprinting, Nanocomposite, Electrostatic interactions, Printing fidelity, Silica nanoparticle

ABSTRACT

3D bioprinting allows the fabrication of 3-dimensional (3D) structures containing living cells whose 3D shape and architecture are matched to a patient. The feature is desirable to achieve personalized treatment of trauma or diseases. However, realization of this promising technique in the clinic is greatly hindered by inferior mechanical properties of most biocompatible bioink materials. Here, we report a novel strategy to achieve printing large constructs with high printing quality and fidelity using an extrusion-based printer. We incorporate cationic

nanoparticles in an anionic polymer mixture, which significantly improves mechanical properties, printability and printing fidelity of the polymeric bioink due to electrostatic interactions between the nanoparticles and polymers. Addition of cationic-modified silica nanoparticles to an anionic polymer mixture composed of alginate and gellan gum results in significantly increased zero-shear viscosity (1062 %) as well as storage modulus (486 %). As a result, it is possible to print a large (centimeter-scale) porous structure with high printing quality, whereas the use of the polymeric ink without the nanoparticles leads to collapse of the printed structure during printing. We demonstrate such a mechanical enhancement is achieved by adding nanoparticles within a certain size range (<100 nm), and depends on concentration and surface chemistry of the nanoparticles as well as the length of polymers. Furthermore, shrinkage and swelling of the printed constructs during crosslinking are significantly suppressed by addition of nanoparticles compared to the ink without nanoparticles, which leads to high printing fidelity after crosslinking. The incorporated nanoparticles do not compromise biocompatibility of the polymeric ink, where high cell viability (> 90%) and extracellular matrix secretion are observed for cells printed with nanocomposite inks. The design principle demonstrated can be applied for various anionic polymer-based systems, which could lead to achievement of 3D bioprinting-based personalized treatment.

INTRODUCTION

Bioprinting has attracted a great deal of attention as a promising technique facilitating direct fabrication of personalized engineered tissue with patient-, and lesion-specific 3D tissue shape and architecture.[1,2] Extrusion-based 3D printing is often preferred for printing cells (i.e. bioprinting) because it can fabricate 3D constructs with clinically relevant sizes in short printing time which is desirable to maintain high cell viability after printing.[2] However, to

achieve high printability and printing fidelity in extrusion-based printing, ink materials should meet certain mechanical properties such as high shear thinning and zero-shear viscosity, and fast shear recovery properties.[2] In addition, ink materials and crosslinking methods have to be biocompatible to obtain desirable biological activities of printed cells and successful tissue regeneration. Various bioinks have been developed by adding rheology modifiers to traditional tissue engineering materials to secure both biocompatibility and printability. For instance, a bioink comprising alginate and gellan gum has been developed where cooling-induced physical gelation of gellan gum provided required shear thinning and recovery properties for printing.[3] The ink allowed 3D printing of various cartilage structures based on 3D digital models and supported chondrogenesis of encapsulated chondrocytes. In addition to gellan gum, gelatin or methacrylated gelatin (GelMA) is another frequently utilized ink component often in combination with alginate to provide some mechanical strength after printing.[4,5] However, polymer-based ink materials often result in only moderate printability, insufficient mechanical strength and/or low printing fidelity due to intrinsic swelling and/or shrinking properties of most polymeric hydrogels.[6,7] In particular, when printing clinically relevant large constructs, inhomogeneous crosslinking due to limited diffusion of crosslinking reagents or transmittance of UV light could result in low printing fidelity, uncontrolled swelling and poor mechanical properties.

Organic/inorganic composite materials have been studied to obtain desirable mechanical properties and gel behaviors for printing.[2,8,9,10] Typically, inorganic particles such as laponite[11,12] and fumed silica[13,14] are added to polymeric solutions to give them a sufficient zero shear viscosity and shear thinning properties. In particular, laponite is utilized intensively for bone tissue engineering and 3D printing due to its unique osteoinductive properties and shear thinning from the “house of cards” structure.[11,12,15] More recently, interactions between

nanoparticles (NPs) and polymers have been actively manipulated to control mechanical properties of nanocomposite hydrogels. Appel et al[16] reported that hydrophobic-modified NPs within the certain diameter range can solely crosslink the polymers with hydrophobic moieties to form a gel via hydrophobic interactions between the NP surfaces and polymers. They reported that the diameter of NPs should be similar to, or smaller than the persistence length of the polymer chain to achieve NP-mediated crosslinking. In the follow-up study, they crosslinked anionic polymers by utilizing the same hydrophobic NPs and a positively charged surfactant which electrostatically interact with both NPs and polymers to crosslink them.[17] In another study, the formation of covalent linkages between magnetic NPs and modified poly(ethylene glycol) resulted in stiff nanocomposite hydrogels at a very low NP concentration.[18] The mechanical properties of nanocomposites were significantly affected by the size of used NPs: a NP dispersion with 8 nm-diameter was found to be the optimal size for mechanical enhancement, which was attributed to the maximum interacting surface area and minimum aggregation of NPs compared to 4 or 12 nm.

Here, we report for the first time that sub-100nm cationic-modified silica NPs can effectively crosslink anionic polysaccharides, which results in high printability and 3D printing fidelity. (**Figure 1A**) Despite of great advantages of solid silica NPs (SiNPs) including control of size, cost, reliability, reproducibility and large-scale production,[19] the use of SiNPs in nanocomposite applications has been limited due to marginal increase in mechanical properties (high viscosity or shear thinning properties) and their limited interactions only with several synthetic polymers such as poly(acrylic acid) or polyacrylamide.[19,20,21] By cationic modification of SiNP surfaces, particles can electrostatically interact with a variety of anionic polysaccharides commonly used in tissue engineering (**Figure 1B**). We hypothesize that 1) cationic SiNPs within a certain size range would reversibly crosslink anionic polymers to

provide shear thinning and recovery properties and 2) addition of cationic SiNPs will suppress swelling of gels by reducing hydrophilicity and thus improve printing fidelity. In fact, addition of cationic SiNPs to a bioink composed of two anionic polysaccharides, alginate and gellan gum, resulted in significant improvement in printability, mechanical strength and printing fidelity.

RESULT

Commercially available LUDOX SiNPs were used as an unmodified, anionic control SiNP and as starting material for aminopropyl-modified aminated cationic SiNPs (AmNPs). After aminopropyl-modification, the size and zeta potential of SiNPs changed from 37.6 nm and -25.8 mV to 41.58 nm and +28.7 mV, respectively (**Table S1**). To confirm the interactions between the AmNPs and polymers, the AmNP dispersion was added to various polymers with different charges. As expected, addition of AmNPs to anionic polymers, heparin (Hep), gellan gum (gellan), chondroitin sulfate (CS), carboxymethylcellulose (CMC), and alginate, resulted in increased turbidity, which indicates formation of polymer-AmNP complexation. (**Figure 1B**) On the other hand, when positively charged polymers (polyethyleneimine (PEI) or chitosan (Chi)) were mixed with AmNPs, the turbidity change was not observed. The NP-polymer complexation was further confirmed by measuring light scattering using a UV-Visible spectrometer, where intensity of scattered light corresponded well to the turbidity changes (**Figure 1C**): significant light scattering was observed for anionic polymers mixed with AmNPs, whereas the light scattering by mixtures of cationic polymers and AmNPs was negligible. The interaction between differently charged NPs and anionic polymers was studied using an alginate solution (2 mg/mL) and SiNPs or AmNPs. The turbidity of the alginate

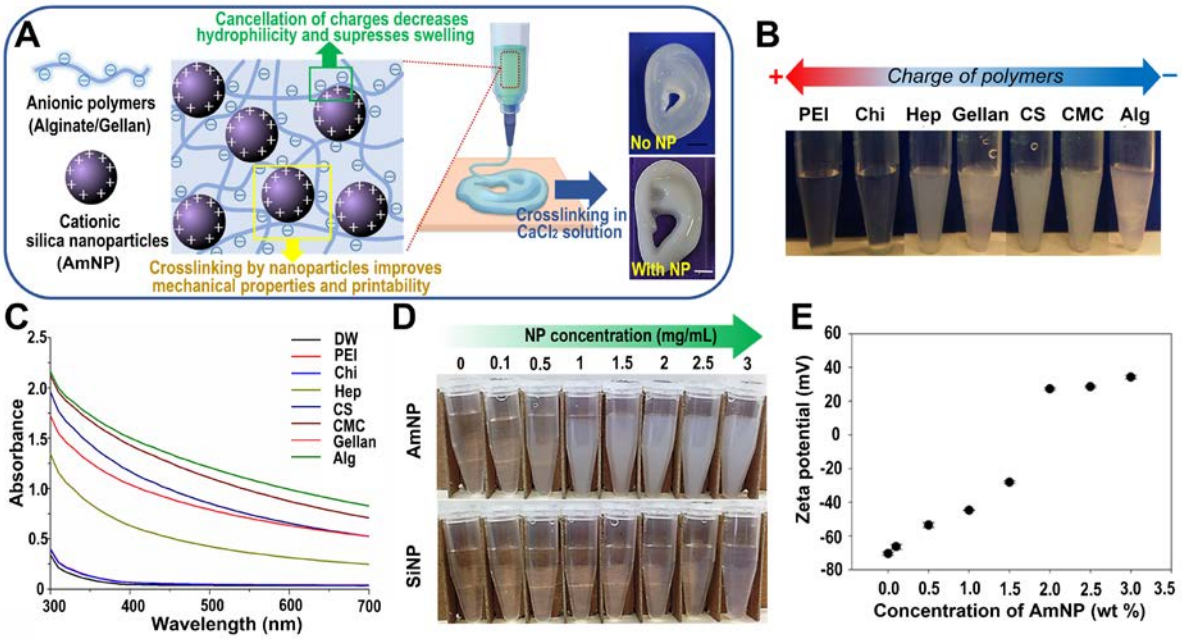

Figure 1. Interaction of NPs with various polymers. A) Schematic presentation of 3D printing utilizing AmNP-based nanocomposite inks. B,C) Photos (B) and UV spectra (C) of mixtures comprising AmNPs and various polymers with different charges. D) Interactions of alginate with AmNPs or SiNPs according to NP concentrations. E) Zeta potentials of alginate solutions mixed with AmNP dispersion with different concentrations.

solution started to change when an AmNP dispersion at 0.5 mg/mL was added, and increased with increasing concentrations of AmNPs. (**Figure 1D**) On the other hand, addition of same or higher amounts of SiNPs (0.5 – 2.5 mg/mL) did not result in any turbidity changes. Lastly, zeta potentials of mixtures composed of alginate and AmNPs were measured. (**Figure 1E**) The zeta potential of an alginate solution was -70.4 mV without AmNPs. The value increased with increasing amounts of AmNPs, and turned positive when the concentration of an added AmNP dispersion was higher than ~2.0 wt%. The result implies that AmNPs electrostatically bind to polymers to form complexation during which charge neutralization occurs.

Nanocomposite inks were prepared by adding NPs to a mixture of two clinically compliant anionic polysaccharides, alginate and gellan. The polymer mixure has been reported as a bioink

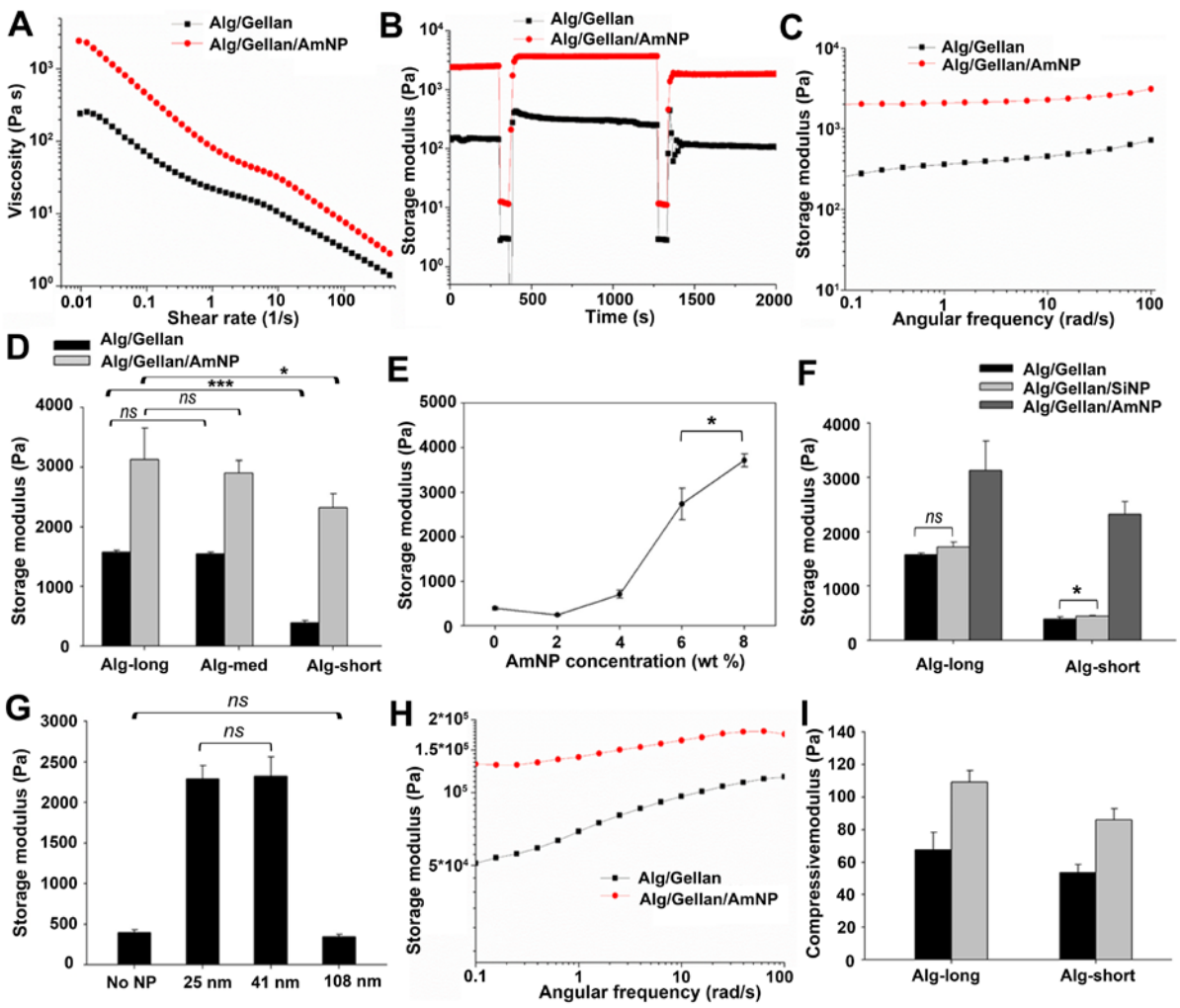

Figure 2. Mechanical properties of inks and crosslinked hydrogels. A-C) Shear thinning (A), shear recovery (B) and storage moduli (C) of Alg/Gellan inks without/with AmNPs. D) Storage modulus of Alg/Gellan inks without/with AmNPs prepared using alginate with different molecular weight (MW). E) Storage modulus of Alg/Gellan inks (Alg-Short) with different amounts of AmNPs. F) Storage modulus of Alg/Gellan inks without NPs, with AmNPs, and with SiNPs. G) Storage modulus of Alg/Gellan inks (Alg-Short) with AmNPs having different diameters. H, I) Storage (H, Alg-Short) and compressive (I, Alg-Short and Long) modulus of Alg/Gellan inks with/without AmNPs after calcium crosslinking for 30 min. *P-value < 0.05; ***P-value < 0.001; *ns:* Not significantly different

where gellan provided shear thinning and recovery properties.[3] Although the polymeric ink was shown to have good printability and biocompatibility, it showed poor printing fidelity after

calcium crosslinking due to swelling and shrinkage of the gel. (**Figure 3D,E**) We prepared inks comprising alginate and gellan without (Alg/Gellan, 3 and 3.5 w/v%, respectively) or with AmNPs (Alg/Gellan/AmNPs). Addition of AmNPs (6 wt%) resulted in significantly enhanced shear thinning (**Figure 2A**) with much higher zero shear viscosity (2,930 Pa s, 1062 % increase) than the Alg/Gellan ink (252 Pa s). A 6 wt% AmNP dispersion alone had very low zero-shear viscosity and hardly exhibited shear thinning properties. (**Figure S1A**) Both Alg/Gellan inks with and without AmNPs exhibited desirable fast shear recovery behaviors although the storage moduli slightly decreased after the second high-strain phase (to 72 % for Alg/Gellan and 85 % for Alg/Gellan/AmNP) compared to the initial values. (**Figure 2B**) In addition, the storage modulus (G', at 1 rad/s) increased by 486 % with AmNPs. (**Figure 2C**) The increased G' was attributed to increased crosslinking density (i.e. decreased pore sizes) by AmNP-mediated crosslinking, which was confirmed by scanning electron microscopy (SEM) analyses (**Figure S2**). The gels with AmNPs had much smaller pore sizes compared to the ones without NPs. We further studied how various factors affect the mechanical properties of the nanocomposites. First, alginates with different MW (**Table S2**) were used to prepare the inks to study the effect of alginate chain lengths on mechanical properties. The storage moduli of Alg/Gellan inks without NPs changed according to the alginate chain length (**Figure 2D**). In particular, when the shortest alginate (Alg-Short) was used, the storage modulus of the ink significantly decreased compared to the others (Alg-Long or Alg-Med). Addition of AmNPs to each ink resulted in enhanced G'. Interestingly, the degree of enhancement was highest for the ink with Alg-Short (485.7 % increase for Alg-Short, 98.5 % increase for Alg-Long). Next, the effect of the concentration of added AmNPs was studied using inks with Alg-Short. (**Figure 2E**) At a low AmNP concentration (2 wt %), no significant change in G' was observed. However, it started to increase when 4 wt% AmNP was added and continued to increase with increasing

AmNP amounts. To study the effect of the NP surface charge on mechanical properties, Alg/Gellan inks with SiNPs or AmNPs were prepared using either Alg-Short or Alg-Long. We did not prepare the ink with Alg-Med because no significant difference was observed between the ink with Alg-Long and Alg-Med. For an Alg/Gellan ink with Alg-Long, addition of SiNPs did not result in significant increase in storage modulus, and the storage modulus of an ink with Alg-Short slightly increased by added SiNPs. (**Figure 2F**) In the SEM analysis, we confirmed that the crosslinking density of an Alg/Gellan with SiNPs was lower than that of the one with AmNPs, where the smaller pore sizes were observed for the gel with AmNPs compared to the one with SiNPs. The result shows that unmodified SiNPs did not crosslink the alginate and gellan as much as AmNPs did. (**Figure S2**)[18,22] The size of NPs was critical for the mechanical strengthening effect of the nanocomposites. Addition of AmNPs with 108 nm in diameter to an Alg/Gellan ink did not result in significant mechanical enhancement. When AmNPs with 25 nm in diameter were added to an Alg/Gellan ink (Alg-Short), the degree of mechanical enhancement was not significantly different from the nanocomposite with AmNP-41 nm. (P-value = 0.866) (**Figure 2G**) Lastly, the mechanical properties of gels after calcium crosslinking were analyzed. The storage modulus increased with addition of AmNPs (**Figure 2H** for Alg-Short, **Figure S1B** for Alg-Long). In addition, ~50 % higher compressive moduli were observed for the nanocomposite gels compared to the polymeric gels (**Figure 2I**). In addition, as we hypothesized, swelling of gels was suppressed with AmNPs, which was confirmed by calculating equilibrium swelling and swelling ratio (**Figure S3**).

Next, printing was performed using an extrusion-based printer to study printability and printing fidelity of the inks. The Alg/Gellan ink prepared using Alg-Short could not be extruded in a continuous uniform strand (**Video S1**) due to its low viscosity. In addition, when printing

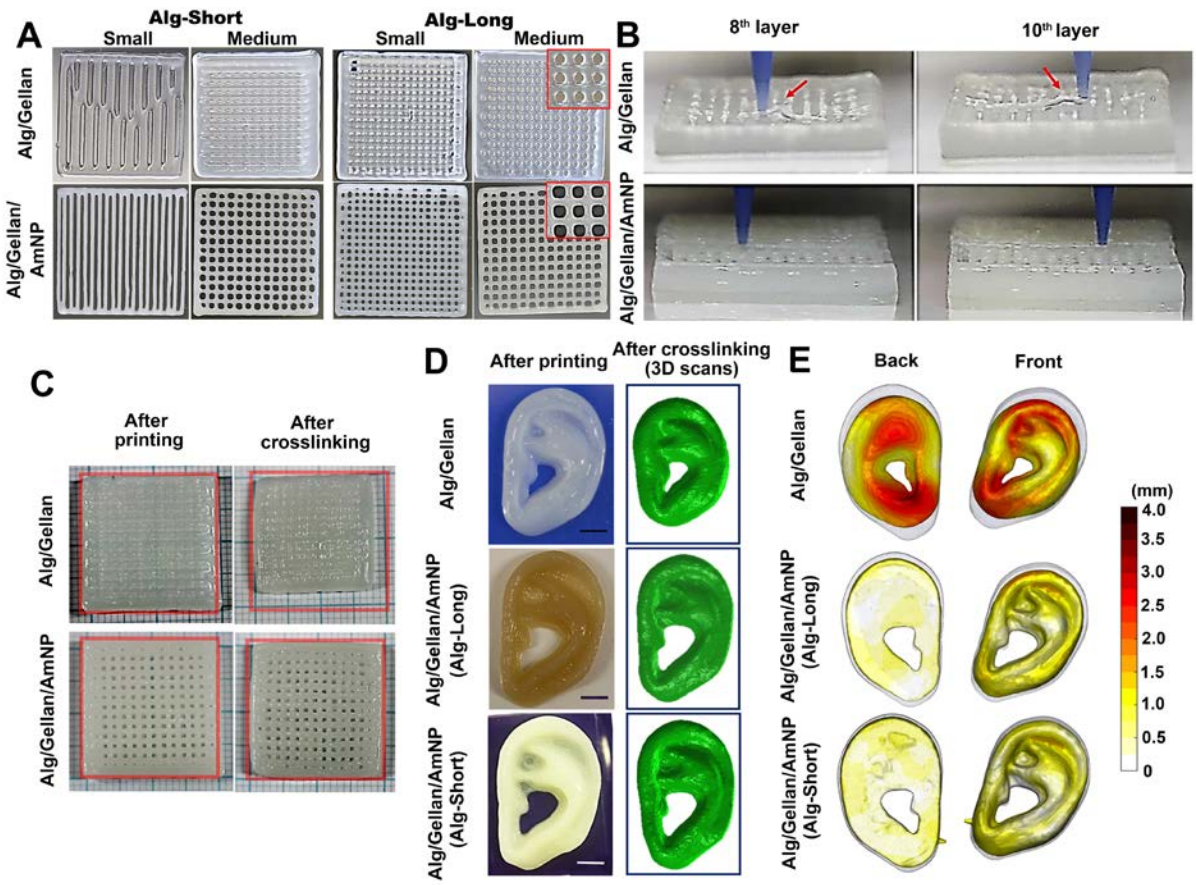

Figure 3. Printability and printing fidelity of prepared inks. A) Left 4 images: Grid structures with small (1 layer) or medium (2 layers) spacing printed using Alg/Gellan inks with/without AmNPs (with Alg-Short). Right 4 images: Grid structures with small (2 layer) or medium (2 layers) spacing printed using Alg/Gellan inks with/without AmNPs (with Alg-Long). B) Printing 8th and 10 th layer using Alg/Gellan inks with/without AmNPs. Red arrows indicate just extruded line that was not properly deposited on the below printed layer due to collapse. C) Images of printed 10-layered grids (2*2 cm) before and after crosslinking. The red boxes have the same size. D) Images of printed ears and 3D scans of printed ears after crosslinking. Bar=5 mm E) Digitalized images of crosslinked ears. The color indicates dimension difference between the printed, crosslinked construct and the original 3D digital model. The grey background is the outline of the 3D design used.

lines with the ink, an extruded line quickly merged to the already printed lines. (**Figure 3A, left**) Addition of AmNPs to the ink dramatically improved its printability: uniform lines could

be continuously extruded (**Video S2**), and the grid structures were maintained with high printing fidelity. Next, printability of an Alg/Gellan ink with Alg-Long was assessed. Although printability of the ink was better than that of the Alg/Gellan ink with Alg-Short, the line-merging phenomena was observed when printing a grid with small spacing so that most of printed pore structures closed during printing. (**Figure 3A, right**) Even when printing a grid with medium spacing, low printing fidelity was observed where the angular pore shape was not kept after printing due to diffusion of the ink at the intersections.[23] With AmNPs in the ink, both line-merging phenomena and ink diffusion at the intersections were greatly suppressed so that both grid structures with small or medium spacing were printed with high fidelity. All printed pores maintained open structures and kept their angular shapes without notable merging or diffusion at the intersection (**Figure 3A**), which was even higher printing fidelity than those of the nanocomposite ink with Alg-Short (**Figure S4**). To further assess the printability, a 10-layered grid structure (**Figure S5A**) was printed. When printing a multi-layered porous structure, some parts of the extruded lines inevitably are printed on air (pore), for which high G' of an ink is highly desirable to prevent collapse of porous structures and achieve high-quality printing.[24] In fact, when the grid was printed using an Alg/Gellan ink, low-quality printing was observed after printing seven layers due to accumulated line-drooping events. (**Figure S5B**) As accumulation of line-drooping events led to significant collapse of the printed construct, the actual height of the printed construct was smaller than the 3D design so that the extruded line was printed on the air instead of the underlying construct. As a result, low-quality printing was observed as indicated by red arrows in **Figure 3B**. On the other hand, with an Alg/Gellan/AmNP ink, the same grid was printed without any collapse, which was attributed to high G' of the Alg/Gellan/AmNP. In addition, for a grid printed using an Alg/Gellan ink, most of pores closed during and after printing due to line-merging phenomena and low-quality

printing, whereas none of pores closed in the grid printed using an Alg/Gellan/AmNP ink. (**Figure 3C, left column**) Furthermore, after crosslinking in a calcium chloride solution, the grid without AmNPs shrank significantly (~10% decrease in length of each side) (**Figure 3C, right column, Figure S5C,D**). However, the grid with AmNPs maintained its dimension without notable shrinkage. Finally, we printed an ear as a clinically relevant, large (centimeter-scale) structure. Based on the same 3D ear model, printing was performed using an Alg/Gellan (Alg-Long) ink with or without AmNPs or Alg/Gellan (Alg-Short) ink with AmNPs. We did not use the Alg/Gellan (Alg-Short) ink without AmNPs because it is not printable as demonstrated above. With all three inks used, ear structures were printed without any pronounced collapse. However, the use of an Alg/Gellan ink without AmNPs resulted in smaller hole in the middle (**Figure 3D**, Top) than the 3D digital design (**Figure S6**), whereas printing with Alg/Gellan/AmNP inks resulted in high printing fidelity. (**Figure 3D**, Middle row & bottom) Furthermore, after 1 hr in crosslinking solution, the ear printed using an Alg/Gellan ink severely shank and swelled, which eventually led to low printing fidelity. In contrast, both swelling and shrinking were greatly suppressed for the ears printed with Alg/Gellan/AmNP inks. (**Figure 3D**) The crosslinked ears were further digitally analyzed to determine the retention of shape. The degree of swelling was presented by the deviation between the 3D design and printed construct. (**Figure 3E**) The degree of swelling varied according to the location in a gel. However, throughout the ear, suppressed swelling was observed for an ear printed using AmNP-containing inks. In addition, even after 1-week incubation in PBS at 37 ^{o}C, higher structural fidelity of ears printed with nanocomposite inks was observed compared to the one printed with the control ink even though all ear structures swelled to a certain degree. (**Figure S7**)

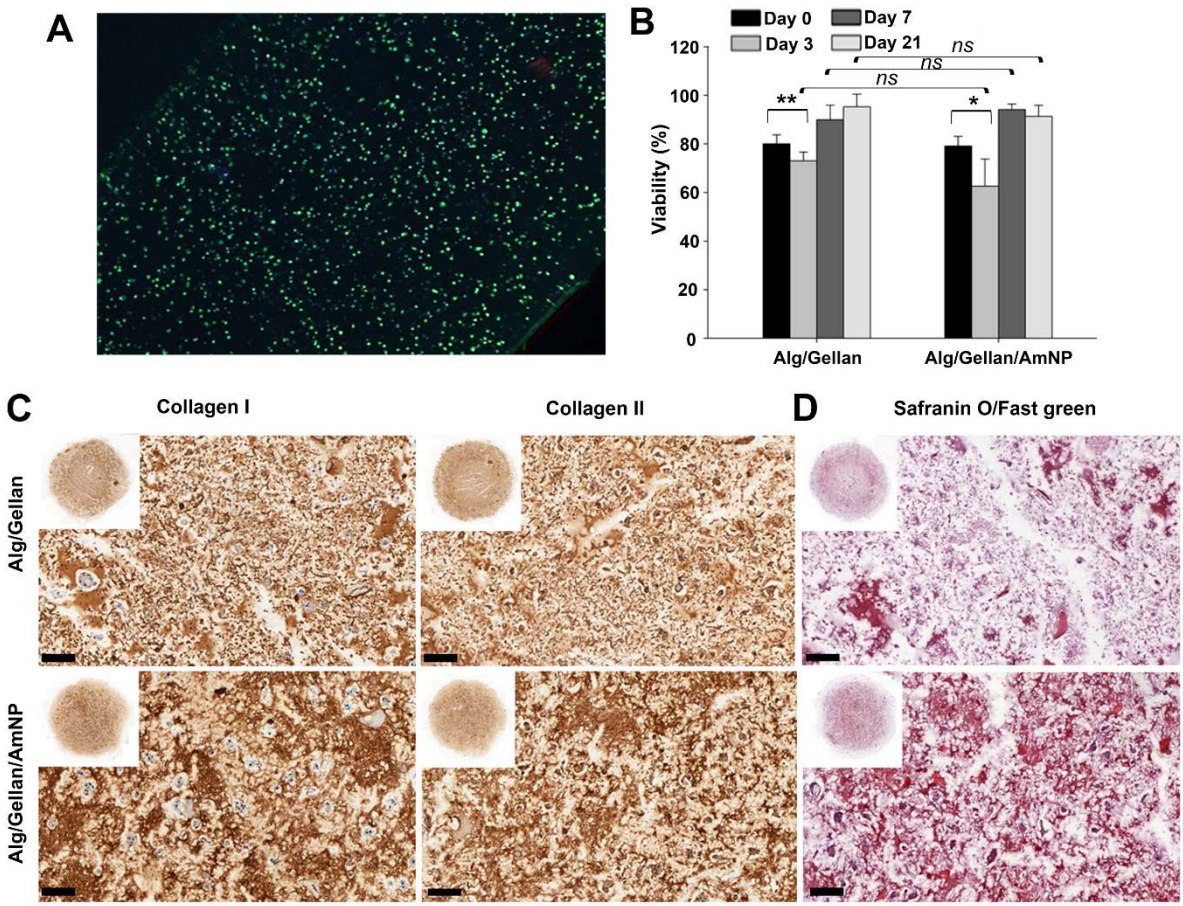

Figure 4. Biocompatibility of the inks. A) Live/dead staining image of printed cells using an Alg/Gellan/AmNP ink. B) Viability of printed cells with an Alg/Gellan or Alg/Gellan/AmNP ink according to culture time. *P-value < 0.05; **P-value < 0.01; *ns:* Not significantly different C) Immunostaining of collagen I and II expressed by printed cells after 6 weeks of in vitro culture. D) Safranin O/Fast green staining of printed cells after 6 weeks of in vitro culture. For all the staining, inks prepared with Alg-Long were used. Bar=100 μm

Lastly, we investigated biocompatibility of the nanocomposite inks. We chose chondrocytes as a cell component considering that cartilage tissue is one of the most targeted tissue in bioprinting research due to its avascularity, a single resident cell type (chondrocytes) and the fact that the function of cartilage is strongly related to its shape.[25] Bovine chondrocytes were isolated from bovine knee articular cartilage and added to each ink. When the cell-containing

inks were casted in a gel caster and crosslinked, the viability for both Alg/Gellan inks (Alg-Long) with and without AmNPs was around ~90 % at day 4. (**Figure S8**) When the same bioinks were printed and crosslinked, the viability at day 0 was comparable to that of casted gels (**Figure 4 A,B**). The viability decreased to 60-70 % at day 3 for both inks, however, it recovered after 1 week of in vitro culture. The printed gels were cultured in chondrogenic media supplemented by TGFβ-3 to confirm the secretion of extracellular matrix by printed chondrocytes. The gels were collected after 6 weeks of culture, and sections immunostained for Collagen I (Col I) and II (Col II). (**Figure 4C, Figure S9 for negative IgG control**) Col II, the main collagen type present in hyaline cartilage,[26] was distributed uniformly throughout a gel, although Col I expression was not efficiently suppressed. Furthermore, we also confirmed uniform expression of glycosaminoglycans (GAGs) by safranin O staining. (**Figure 4D**) When the nanocomposite ink with Alg-Short was used for printing cells, uniform and intense expression of collagens and GAGs was observed (**Figure S10**) similar to the results of the inks with Alg-Long. The results show that the presence of the AmNPs in a gel does not compromise the matrix secretion by cells.

DISCUSSION

Addition of cationic NPs to an anionic polymer mixture led to significant mechanical enhancement in terms of shear thinning properties, zero-shear viscosity, G' and mechanical strength after crosslinking, which is attributed to reversible, electrostatic crosslinking of polymers by the NPs. We demonstrated such a mechanical enhancement by AmNPs is affected by several different factors. An Alg/Gellan with Alg-Short exhibited lower G' compared to an Alg/Gellan with Alg-Long. Interestingly, when AmNPs were added to the ink with Alg-Short, the G' increased by 485.7 % which is much higher enhancement compared to the ink with Alg-

Long. According to a previous study,[27] the observed difference in mechanical enhancement between two inks could be because the *number of polymer chains adsorbed by a particle* (***N***) decreases with increasing polymer MW due to larger free adsorption site on a longer polymer chain. In the study, G' of a composite gel composed of poly(ethylene oxide) and laponite decreased with increasing MW of poly(ethylene oxide). In addition, several studies[18,28] suggested that mechanical enhancement by NPs in a composite material is possibly because NPs act as 'crosslink epicenters' which bring multiple polymer chains to one point (surface of a NP) and connect them. Therefore, the higher ***N*** number implies more efficient crosslinking by a NP. Furthermore, another study reported that the longer polymer chain is used in a nanocomposite, the more aggregations are induced due to the weaker interaction with NPs.[29] Indeed, we experienced more clogging for the ink with Alg-Long and AmNPs compared to the one with Alg-Short and AmNPs. When agglomeration is induced in a composite, the number of NPs with effective interacting surface area is reduced, which would lead to reduced interactions between NPs and polymers and thus decreased mechanical enhancement.[18] Therefore, we conclude that the higher degree of mechanical enhancement of the ink with Alg-Short possibly results from both the higher *N* number and less agglomeration compared to the ink with Alg-Long. In addition to the MW of alginate, the surface functionality of NPs greatly affected the mechanical property, where addition of unmodified SiNPs to polymers resulted in only slightly increased G'. In general, SiNPs are known to interact with certain synthetic polymers via hydrogen bond formation. [20,21] However, for polysaccharides, no such a significant interaction has been reported, and we also confirmed that addition of SiNPs did not have significant impact on mechanical properties of the Alg/Gellan. Thus, the result strongly implies the observed mechanical enhancement by AmNPs is attributed to strong electrostatic interactions between anionic polymers and cationic AmNPs as we hypothesized. The size of

NPs was another critical factor which affected mechanical properties of the nanocomposite inks. Addition of AmNPs larger than 100 nm did not result in any enhancement in G', which is probably because such a large particle does not provide sufficient interacting surface area required for mechanical enhancement. In addition, when the diameter of NPs is too large compared to the persistence lengths of polymers in the nanocomposite, the NPs cannot be bridged by a polymer strand but are rather coated by polymers.[16] Considering the reported persistence lengths of alginate (~15 nm [30]) and gellan (9.4 - 98 nm depending on the temperature [31]), the NP with 108 nm in diameter would likely induce surface coating by polymers rather than crosslinking. No significant difference in G' was observed between Alg/Gellan/AmNP inks prepared using AmNPs with 25 or 41 nm. Although the smaller particle (25 nm) has the larger interacting surface area than the larger one (41 nm), the smaller particle also has higher tendency to aggregate.[18] Thus, the actual interacting surface area of the smaller particles is possibly reduced by aggregation.

The mechanical enhancement by added AmNPs led to significantly improved printability and printing fidelity. The ink with AmNPs allowed printing small spacing grid structures with high printing quality, which means the printing resolution is improved. In addition, when printing a medium spacing grid structure with an Alg/Gellan ink, the printed angular pore structure was quickly lost due to diffusion of the ink at the intersections.[23] (**Figure 3A, right, inset**) In contrast, the use of an Alg/Gellan/AmNP ink for printing the same structure resulted in high shape fidelity. (**Figure 3A, right, inset**) Furthermore, an ink with AmNPs enabled printing of a tall (10 layer), porous structure without collapse of underlying strands. A material with high yield stress can maintain the straight filament shape on the air better without collapse than the material with low yield stress.[24] (**Figure S5B**) Thus, printing the tall structure using the ink without AmNPs which has low yield stress (10.8 Pa) resulted in low-quality printing

after printing ~7 layers due to collapse of the printed layers. In contrast, the nanocomposite ink (yield stress of 51.4 Pa) exhibited much better printability without notable collapse. In addition to printability, the printing fidelity was greatly improved with AmNPs where swelling and shrinking of printed gels were suppressed during crosslinking. Suppressed swelling is attributed to higher crosslinking density (**Figure S2**) as well as decreased hydrophilicity[32] which was confirmed by increased zeta potentials of alginate solutions with AmNP additions. (**Figure 1D**) Suppression of shrinkage by AmNPs improved printing fidelity of printed constructs after crosslinking. (**Figure 3C,E**) The observed shrinkage for Alg/Gellan gels is possibly due to swelling of the gel in the vertical direction. (**Figure S5E, Figure 3E**) Rapid, diffusion-driven calcium crosslinking of Alg/Gellan gels led to formation of a shell-like layer near the gel surface, (**Figure S11**) which resulted from efficient ion diffusion at the gel surface and thus high crosslinking density.[33,34] The highly crosslinked shell structure could physically limit the swelling-driven volume expansion of the gel, and thus, the vertical volume expansion (swelling) could lead to shrinkage in the horizontal direction for a given volume of the gel. We observed that printed constructs with higher degree of swelling such as a small spacing multi-layered grid or large ear structure tended to shrink in a greater extent compared to gels with lower swelling. For gels with AmNPs, thus, the shrinkage was suppressed possibly due to suppressed swelling. The exact mechanism of the gel-shrinkage, however, should be further studied.

For both inks with/without AmNPs, reduced viability of printed cells was observed at day 3. (**Figure 4B**) Considering that the 'day 0' test was performed right after the printing and crosslinking, it seems that some of cells damaged during printing[9] eventually died and were detected at day 3. However, no significant difference between two inks was observed at day 3. In addition, the viability recovered the level higher than 90 % after 1 week of culture for both

gels. More importantly, the uniform expression of collagens and GAGs was confirmed for both gels. (**Figure 4C, D**) Safranin O is a cationic dye that stains negatively charged GAGs in tissue via electrostatic adsorption. Thus, the dye also stained the gels even without cells but less intensively compared to the gels with cells. (**Figure S12**) In addition, the intensity of the background staining was significantly lower for the ink with AmNPs than the one without AmNPs possibly due to reduced negative charges in the gel with AmNPs.

CONCLUSION

We demonstrated that addition of cationic NPs to anionic polymeric bioinks greatly enhanced printability during printing, and printing fidelity and mechanical strength after crosslinking. In particular, the cationic NPs efficiently suppressed swelling and shrinking behaviors of printed gels, which is attributed to decreased hydrophilicity and high crosslinking density of the NP-containing gels. In addition, the nanocomposite gels supported the growth and extracellular matrix secretion of printed chondrocytes as much as the control gels did. Considering that many of tissue engineering and bioprinting systems utilize anionic polysaccharides such alginate and hyaluronic acid, the design principle incorporating cationic NPs could be extensively applied to various systems and be a key component of advanced materials in tissue engineering and personalized regenerative medicine.

EXPERIMENTAL SECTION

Preparation of inks All inks were prepared in a solution containing 300 mM glucose (Sigma-Aldrich) and 20 mM (4-(2-hydroxyethyl)-1-piperazineethanesulfonic acid) (HEPES, Sigma-Aldrich) at pH 7.4. To prepare a control ink, alginate and gellan powder were added to the

solution followed by magnetic stirring at 90 ^{o}C and 300 rpm for 1 h. Then, the mixture was taken from the oil bath and vigorously mixed with a spatula until it cooled down to RT. To remove agglomerations, the ink was post-processed using two-syringes connected to each other by a lure connector with a small homogenizing screw (Medmix Systems AG, Risch-Rotkreuz, Switzerland). The ink was passed through the connector back and forth for 5 min. Finally, the ink was centrifuged at 3000 rpm for 30 min to remove air bubbles. Inks containing SiNPs or AmNPs were prepared according to the same method described above but NPs were added to the Glucose/HEPES solution at typically 6 wt% prior to additions of polymer powder. All inks were used for mechanical testing and printing within 7 days.

Mechanical testing Rheology of all inks and gels were characterized using a rheometer (MCR 301, Anton Paar, Zofingen, Switzerland) with a flat plate geometry (diameter of 20 mm for inks and 10 mm for gels) at 25 ^{o}C. The measuring chamber was saturated by water vapor to prevent samples from drying. For assessing shear thinning properties, viscosity of an ink was measured in a range of shear rate (0.01 – 500 1/s) with a gap of 0.5 mm. In a shear recovery test, storage (G') and loss (G") modulus were recorded at a frequency of 1 Hz for an ink exposed to mechanical cycles as follows: at 0.5% strain for 200 s – at 1000 % strain for 10 s – at 0.5% strain for 600 s – at 1000 % strain for 10 s – at 0.5% strain for 600 s. To measure storage modulus, a frequency sweep test was done with 0.07 % strain and in a range of frequency (100 – 0.1 rad/s). The strain used for the frequency sweep test was determined within the linear viscoelastic (LVE) range by an amplitude sweep test. Compression test for gels was performed using a texture analyzer (TA.XT plus, Stable Micro Systems). For that, an ink (50 μl) was casted in a gel caster with 1 mm thickness and crosslinked in a crosslinking solution ($CaC1_2$ 100 mM, NaCl 70 mM) for 30 min. Afterwards the gel was cut into 6 mm using a biopsy punch. The compressive test was performed with a probe speed of 0.01 mm/s until 25%-

strain is reached. The young's modulus was calculated from a slope of the resultant stress-strain curve in a linear region (5-10 %, R^2>0.99).

3D printing Design of 3D objects was done with software, Autodesk Fusion 360. G-codes were created using Slicer software based on created 3D object files (.stl). Printing acellular constructs was performed using an extrusion-based 3D printer from Cellink (INKREDIBLE, Gothenburg, Sweden). The typical printing pressure ranges were 35-40kPa for the control ink and 40 – 50 kPa for inks with AmNPs. A needle with a diameter of 410 μm was used for all printing. The printing speed was controlled in the range of 10 – 20 mm/s. For printing cells, another extrusion-based 3D printer (Biofactory, RegenHu, Switzerland) installed in a sterile hood was used, but other printing conditions were controlled in the same range used for the INKREDIBLE printer. To prepare cell-containing inks, a cell suspension with $1*10^8$ cells/mL was added to an ink at 1:9 (v/v) followed by gentle mixing with a spatula. The ink was then loaded to a printing syringe and used for printing. After printing, printed constructs were crosslinked in the crosslinking solution with gentle shaking (70 rpm) for 1 h. For the swelling tests, the crosslinked ears were transferred to a tube filled with 20 mL PBS, and incubated at 37 ^{o}C for 7 days.

Image analysis For digital analyses, the ears were scanned using a 3D scanner (Mono scan, Smart optics sensortechnik GmbH, Bochum, Germany). In order to estimate the point-wise shape deviation between the 3D digital design of the ear (reference triangular mesh model R) and the 3D scan of a printed construct (triangular mesh model P), it was necessary to obtain a dense correspondence between their surfaces via a non-rigid registration process where the reference model R is deformed. First, 20 landmarks were defined over the surface of R, and their counterpart points were picked over the surface of P. Based on these 20 pairs of points, a Procrustes analysis lead to the rigid alignment of R on P, resulting in R0. The same landmarks

were then used as the control points of a Thin-Plate Spline deformation,[4] resulting in R1. The vertices of the warped model R1 were then projected onto the surface of P, and used as target points in a smooth deformation stage involving the mesh Laplacian (Laplacian surface editing[5]) and resulting in R2. The mesh R3 was finally obtained as the projection of R2 onto P, thus providing the desired dense correspondence : the point-wise shape deviation was derived as the Euclidean distance between the vertices of R0 and their counterpart in R3

Cell culture and viability test All reagents for cell culture and staining were purchased from Life Technologies (Zug, Switzerland) unless stated otherwise. Chondrocytes were isolated from bovine knee cartilages. For the isolation, firstly, pieces of cartilages were collected from a bovine knee cartilage and minced into small pieces (<1*1*1 mm). The minced cartilage was treated with collagenase (9.6 mg pear 1 g cartilage) at 37 ^{o}C with mild shaking for 5 h. Afterwards cells were collected by filtering them through a sieve with a mesh size of 100 μm followed by centrifugation at 250 g for 8 min. The cell pellet was dispersed in a culture medium and washed once followed by centrifugation at 250 g for 6 min. Finally the cells were frozen in a recovery media and stored in liquid nitrogen. For viability test, cells were expanded to passage 3 in a culture medium (No.31966) supplemented with fetal bovine serum (FBS), gentamycin 10 μg/mL, and ascorbic acid (Sigma-Aldrich) 50 μg/mL. The cells were added to each ink at 1:9 (v/v), and the cell-containing ink was either casted or printed followed by crosslinking for 30 min. The gels were incubated at 37 ^{o}C and 5 % CO_2 for 0, 3, 7, or 21 days. For live/dead staining, gels were collected at each time point, washed twice with PBS, and incubated in a staining solution containing calcein-AM (2 μM) and propidium iodide (5.88 μg/mL, Sigma-Aldrich) in PBS for 30 min. Afterwards the gels were washed with PBS and imaged using a microscope (Axio Observer, Carl Zeiss, Oberkochen, Germany).

ACKNOWLEDGEMENT

This work was financially supported by a starting grant from CABMM and the Swiss National Science Foundation (CRSII5_173868).

CONFLICT-OF-INTEREST DISCLOSURE

Marcy Zenobi-Wong is a consultant for Auregen Biotherapeutics AG.

SUPPORTING INFORMATION

Additional experimental details, tables displaying zeta potentials/sizes of NPs and MWs of alginates, additional rheology data, SEM images of gels, plots showing equilibrium swelling and swelling ration of gels, additional photos of printed grids, photos of crosslinked printed girds, images of 3D digital models of the ear and grid, photos of printed ears after 1-week incubation in PBS, viability of cells in casted gels, additional histology data (PDF) and videos demonstrating extrusion of inks.

REFERENCES

1. Moroni, L.; Boland, T.; Burdick, J. A.; Maria, C. D.; Derby, B.; Forgacs, G.; Groll, J.; Li, Q.; Malda, J.; Mironov, V. A.; Mota, C.; Nakamura, M.; Shu, W.; Takeuchi, S.; Woodfield, T. B. F.; Xu, T. Yoo, J. J.; Vozzi. G. Biofabrication: A Guide to Technology and Terminology. *Trends Biotechnol.* **2018**, *36*, 384.

2. Jungst, T.; Smolan, W.; Schacht, K.; Scheibel, T.; Groll, J. Strategies and Molecular Design Criteria for 3D Printable Hydrogels. *Chem. Rev.* **2016,** *116*, 1496-1539.

3. Kesti, m.; Eberhardt, C.; Pagliccia, G.; Kenkel, D.; Grande, D.; Boss, A.; Zenobi-Wong, M. Bioprinting Complex Cartilaginous Structures with Clinically Compliant Biomaterials. *Adv. Funct. Mater*. **2015,** *25*, 7406-7417.

4. Wu, Z.; Su, X.; Xu, Y.; Kong, B.; Sun, W.; Mi, S.; Bioprinting Three-Dimensional Cell-Laden Tissue Constructs with Controllable Degradation. *Sci. Rep.* **2016,** *6*, 24474.

5. Yin, J.; Yan, M.; Wang, Y.; Fu, J.; Suo, H. 3D Bioprinting of Low-Concentration Cell-Laden Gelatin Methacrylate (GelMA) Bioinks with a Two-Step Cross-linking Strategy. *ACS Appl. Mater. Interfaces* **2018,** *10*, 6849-6857.

6. Caliari, S. R.; Burdick, J. A. A Practical Guide to Hydrogels for Cell Culture. *Nat. Methods* **2016,** *13* (5), 405-414.

7. Billiet, T.; Vandenhaute, M.; Schelfhout, J.; Vlierberghe, S. V.; Dubruel, P. A Review of Trends and Limitations in Hydrogel-Rapid Prototyping for Tissue Engineering. *Biomaterials* **2012,** *33*, 6020-6041.

8. Luo, Y.; Wu, C.; Lode, A.; Gelinsky, M. Hierarchical Mesoporous Bioactive Glass/Alginate Composite Scaffolds Fabricated by Three-Dimensional Plotting for Bone Tissue Engineering. *Biofabrication* **2013,** *5*, 015005.

9. Muller, M.; Ozturk, E.; Arlov, Ø.; Gatenholm, P.; Zenobi-Wong, M. Alginate Sulfate–Nanocellulose Bioinks for Cartilage Bioprinting Applications. *Ann. Biomed. Eng.* **2016,** *45*, 210-223.

10. Shin, S.; Park, S.; Park, M.; Jeong, E.; Na, K.; Youn, H. J.; Hyun, J. Cellulose Nanofibers for the Enhancement of Printability of Low Viscosity Gelatin Derivatives. *BioResources* **2017,** *12*, 2941-2954.

11. Jin, Y.; Lui, C.; Chai,W.; Compaan, A.; Huang, Y. Self-Supporting Nanoclay as Internal Scaffold Material for Direct Printing of Soft Hydrogel Composite Structures in Air. *ACS Appl. Mater. Interfaces* **2017,** *9*, 17456-17465.

12. Chimene, D.; Peak, C. W.; Gentry, J. L.; Carrow, J. K.; Cross, L. M.; Mondragon, E.; Cardoso, G. B.; Kaunas, R.; Gaharwa, A. K. Nanoengineered Ionic−Covalent Entanglement (NICE) Bioinks for 3D Bioprinting. *ACS Appl. Mater. Interfaces* **2018,** *10*, 9957-9958.

13. Zhu, C.; Han, T. Y. -J.; Duoss, E. B.; Golobic, A. M.; Kuntz, J. D.; Spadaccini, C. M.; Worsley, M. A. Highly compressible 3D periodic graphene aerogel microlattices. *Nat. Commun.* **2015,** *6*, 6962.

14. Mishra, S.; Scarano F. J.; Calvert, P. Rapid Prototyping of Three-Dimensional Nanocomposite Hydrogel Constructs: Effect of Silica Nanofiller on Swelling and Solute Release Behaviors of the Nanocomposite Hydrogels. *J. Biomed. Mater. Res. PartA* **2015,** *103*, 3237-3249.

15. Gaharwar, A. K.; Mihalia, S. M.; Swami, A.; Patel, A.; Sant, S.; Reis, L. R.; Marques, A. P.; Gomes, M. E.; Khademhosseini, A. Bioactive Silicate Nanoplatelets for Osteogenic Differentiation of Human Mesenchymal Stem Cells. *Adv. Mater.* **2013,** *25*, 3329-3336.

16. Appel, E. A.; Tibbitt, M. W.; Webber, M. J.; Mattix, B. A.; Veiseh, O.; Langer, R. Self-Assembled Hydrogels Utilizing Polymer–Nanoparticle Interactions. *Nat. Commun.* **2015,** *6*, 6295.

17. Appel, E. A.; Tibbitt, M. W.; Greer, J. M.; Fenton, O. S.; Kreuels, K.; Anderson, D. G.; Langer, R. Exploiting Electrostatic Interactions in Polymer−Nanoparticle Hydrogels. **2015,** *4*, 848-852.

18. Jaiswal, M. K.; Xavier, J. R.; Carrow, J. K.; Desai, P.; Alge, D.; Gaharwar, A. K. Mechanically Stiff Nanocomposite Hydrogels at Ultralow Nanoparticle Content. *ACS Nano* **2016,** *10*, 246-256.

19. Rahman, I. A.; Padavettan, V. Synthesis of SilicaNanoparticles by Sol-Gel: Size-Dependent Properties, SurfaceModification, and Applications in Silica-PolymerNanocomposites—A Review. *J. Nanomater.* **2012,** *2012*, 132424.

20. Yanga, J.; Shi, F.-K.; Gonga, C.; Xie, X.-M.; Dual Cross-Linked Networks Hydrogels with Unique Swelling Behavior and High Mechanical Strength: Based on Silica Nanoparticle and Hydrophobic Association. *J. Colloid. Interface Sci.* **2012,** *381*, 107-115.

21. Wang, Q.; Hou, R.; Chenga, Y.; Fu, J. Super-Tough Double-Network Hydrogels Reinforced by Covalently Compositing with Silica-Nanoparticles. *Soft Matter* **2012,** *8*, 6048-6056.

22. Maia, J.; Ferreira, L.; Carvalho, R.; Ramos, M. A.; Gil, M. H. Synthesis and Characterization of New Injectable and Degradable Dextran-Based Hydrogels. *Polymer* **2005,** *46*, 9604–9614.

23. He, Y.; Yang, F. F.; Zhao, H. M.; Gao, Q.; Xia, B.; Fu, J. Z.; Research on the Printability of Hydrogels in 3D Bioprinting. *Sci. Rep.* **2016,** *6*, 29977.

24. Ribeiro, A.; Blokzijl, M. M.; Levato, R.; Visser, C. W.; Castilho, M.; Hennink, W. E.; Vermonden, T.; Malda, J. Assessing Bioink Shape Fidelity to Aid Material Development in 3D Bioprinting. *Biofabrication* **2018,** *10*, 014102.

25. Bella, C. D.; Fosang, A.; Donati, D. M.; Wallace, G. G.; Choong, P. F. M. 3D Bioprinting of Cartilage for Orthopedic Surgeons: Reading between the Lines. *Front. Surgery* **2015,** *2*, 39.

26. Bhosale, A. M.; Richardson, J. B. Articular Cartilage: Structure, Injuries and Review of Management. *Br. Med. Bull.* **2008,** *87*, 77-95.

27. Can, V.; Okay, O. Shake Gels Based on Laponite–PEO Mixtures: Effect of Polymer Molecular Weight. *Des. Monomers Polym.* **2005,** *8*, 453-462.

28. Li, Q.; Barrett, D. G.; Messersmith, P. B.; Holten-Andersen, N. Controlling Hydrogel Mechanics via Bio-Inspired Polymer−Nanoparticle Bond Dynamics. *ACS Nano* **2016,** *10*, 1317-1324.

29. Smitha, J. S.; Bedrova, D.; Smith, G. D. A Molecular Dynamics Simulation Study of Nanoparticle Interactions in a Model Polymer-Nanoparticle Composite. *Compos. Sci. Technol.* **2003,** *63*, 1599-1605.

30. Vold, I. M. N.; Kristiansen, K. A.; Christensen, B. E. A Study of the Chain Stiffness and Extension of Alginate, in Vitro Eprmerized Alginates, and Periodate-Oxidized Alginates Using Size-Excluion Chromatogaphy Combined with Light Scattering and Viscosity Detectors. *Biomacromol*. **2006**, *7*, 2136-3146.

31. Takahashi, R.; Tokunou, H.; Kubota, K.; Ogawa, E.; Oida, T.; Kawase, T.; Nishinari, K. Solution Properties of Gellan Gum: Change in Chain Stiffness between Single- and Double-Stranded Chains. *Biomacromol*. **2004**, *5*, 516-523.

32. Miyata, T.; Jikihara, A.; Nakamae, K. Preparation of Poly(2-glucosyloxyethyl methacrylate)-Concanavalin A Complex Hydrogel and its Glucose-Sensitivity. *Macromol. Chem. Phys.* **1996,** *197*, 1135 -1146

33. Thu, B.; Gaserod, O.; Paus, D.; Mikkelsen, A.; Skjåk-Bræk, G.; Toffanin, R.; Vittur, F.; Rizzo, R. Inhomogeneous Alginate Gel Spheres: An Assessment of the Polymer Gradients by Synchrotron Radiation-Induced X-Ray Emission, Magnetic Resonance Microimaging, and Mathematical Modeling. *Biopolymers* **2000,** *53*, 60-71.

34. Boland, T.; Xu, T.; Damon, B.; Cui, X. Application of Inkjet Printing to Tissue Engineering. *Biotechnol. J.* **2006** *1*,910–917.
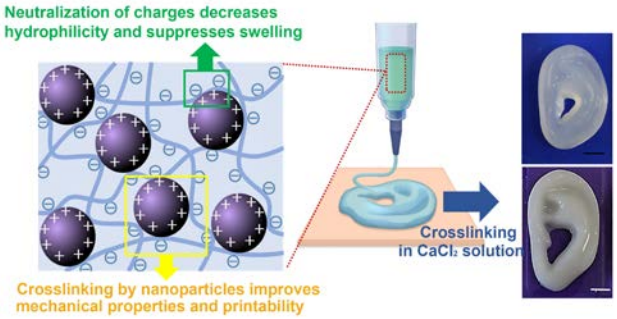
Graphical Table of Contents.